# A Model Analysis of the Thermal Conductivity of Ag-doped Bi–Sr–Ca–Cu–O Superconducting Oxide



1994 Jpn. J. Appl. Phys. 33 2004

(http://iopscience.iop.org/1347-4065/33/4R/2004)

Jpn. J. Appl. Phys. Vol. 33 (1994) pp. 2004–2007
Part 1, No. 4A, April 1994

# A Model Analysis of the Thermal Conductivity of Ag-doped Bi–Sr–Ca–Cu–O Superconducting Oxide

Manabu IKEBE, Hiroyuki FUJISHIRO, Michiaki MATSUKAWA, Fumiaki TATEZAKI, Hiromitsu OGASAWARA, Koshichi NOTO, Kazuo MICHISHITA[1] and Yukio KUBO[1]
*Faculty of Engineering, Iwate University, 4-3-5 Ueda, Morioka 020*
[1]*Japan Fine Ceramics Center, 2-4-1 Mutsuno, Atsuta, Nagoya 456*

(Received November 8, 1993; acceped for publication January 22, 1994)

A phenomenological model to analyze the transport phenomena in inhomogeneous materials is proposed and applied to the measured thermal conductivity of Ag-doped Bi–Sr–Ca–Cu–O (Bi2212) superconducting oxide. Based on the model, the effective ratios of the doped Ag amount in the grain boundary to that inside of the grain are determined to be 0.75:1.0 for a Bi2212+15 wt% Ag specimen and 0.85:1.0 for a Bi2212+10 wt% Ag specimen. The model analyses indicate that doped Ag particles preferentially occupy the grain boundaries, contributing to the formation of the linked Ag heat path in the oxides.

KEYWORDS: Ag-doped Bi2212 superconductor, floating zone method, improved weak link, macroscopic inhomogeneity, thermal conductivity, generalized heat circuit

## 1. Introduction

A variety of composite and complex materials have been devised to realize desired performance in practical-use. The addition of Ag to the oxide superconductors is known to improve superconducting properties, such as the critical current $J_c$.[1-3] The origin of the $J_c$ enhancement is believed to be due to the doped Ag particles which are located at the grain boundaries and enhance the coupling between the superconducting grains.[4-6] Ag doping is expected to affect the transport properties in both superconducting and normal states. Heat conduction is an important factor in cryogenic engineering because the stable operation of cryogenic equipment is determined by thermal conduction and diffusion. In this paper, the conductivity data of Ag-doped Bi–Sr–Ca–Cu–O (Bi2212) compounds[6] are examined using a simple phenomenological model. The model allows us to determine the Ag contents in the grain boundaries and inside of the grains.

## 2. Experimental

The Bi2212 bulk samples doped with 10 wt% and 15 wt% Ag and without Ag doping were prepared by a floating zone (FZ) method at Japan Fine Ceramics Center (JFCC).[7-9] The FZ method provides an aligned crystal structure with the ab-plane parallel to the growth direction. The Ag-doped FZ samples also show a textured structure with the $c$-axis of grains nearly parallel to each other. The sample dimensions for the thermal conductivity measurement were typically $\approx 2 \times 2 \times 15$ mm$^3$.

The thermal conductivity was measured at temperatures between 15 K to 200 K by a steady-state heat flow method. One end of the sample was attached by indium solder to a copper block on the cold head of the Gifford-McMahon cycle helium refrigerator. A metal film resistor was attached as a heater to another end of the sample using GE7031 varnish. The temperature difference between two terminals (distance $\approx 8$ mm) on the sample was monitored by the differential thermocouple (Au+0.07 at.% Fe+Chromel). The absolute temperature of the sample was monitored by another thermocouple. The heat flow was applied in the direction parallel to the ab-plane of the Bi2212 crystal lattice (in-plane conductivity). The detailed method of the thermal conductivity measurement has already been described elsewhere.[6,10]

## 3. Results and Discussion

The superconductive transition temperature $T_c$ of the present FZ samples was determined resistively. The results of the electrical resistivity are summarized in Table I. Figure 1 shows the temperature dependence of the thermal conductivity $\kappa(T)$ of Bi2212 samples with and without Ag doping. $\kappa(T)$ of the undoped sample (#00A) shows gradual and monotonic decrease with decreasing temperature. We did not observe the upturn of $\kappa(T)$ near $T_c$ usually associated with the onset of superconductivity.[11-13] The absence of the upturn might suggest that the FZ samples have an inhomogeneous nature from the view point of superconductivity. In Fig. 1, the thermal conductivities of both 10 wt% Ag doped sample (#10A) and 15 wt% Ag doped sample (#15A) are enhanced compared to that of undoped #00A. The enhancement becomes more remarkable with increasing Ag concentration. $\kappa(T)$ of #10A and #15A also shows gradual decrease with lowering of temperature down to $\approx 100$ K, which is in qualitative agreement with $\kappa(T)$ of #00A. The conductivities of #10A and #15A, however, show a broad minimum around 80–100 K. $\kappa(T)$ of #15A drastically increases below 50 K, takes a maximum at about 23 K and sharp-

Table I. Electrical resistivity of the samples and Ag+Au alloys.

| Sample | $T_{cend}$ (K) | Resistivity (at 4.2 K) | Resistivity (at 280 K) | *RRR* |
|---|---|---|---|---|
| Bi2212 | 86.3 | — | 0.75 mΩ·cm | — |
| Bi2212+10 wt% Ag | 93.6 | — | 0.25 mΩ·cm | — |
| Bi2212+15 wt% Ag | 93.1 | — | 0.15 mΩ·cm | — |
| Ag+0.085 at.% Au | — | 0.04 μΩ·cm | 1.47 μΩ·cm | 37 |
| Ag+0.22 at.% Au | — | 0.10 μΩ·cm | 1.51 μΩ·cm | 15 |

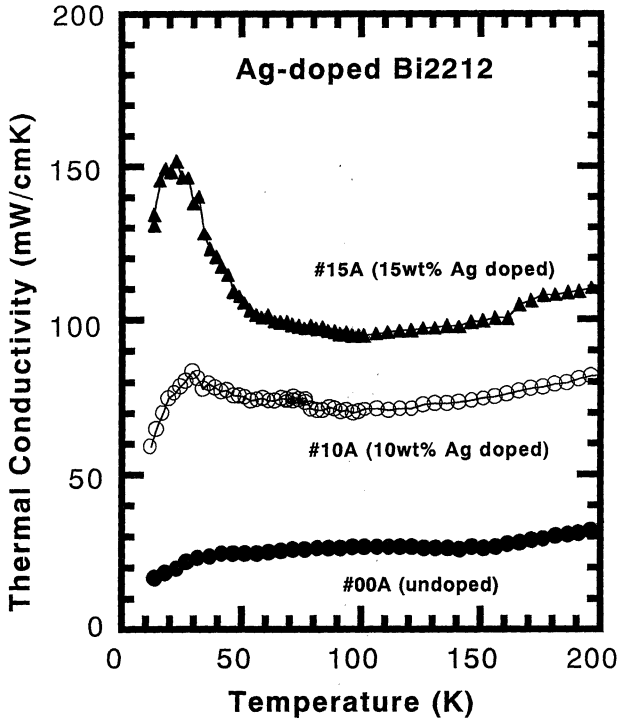


Fig. 1. The temperature dependence of the thermal conductivity of Bi2212 samples with and without Ag doping. Samples are prepared by a floating zone method.

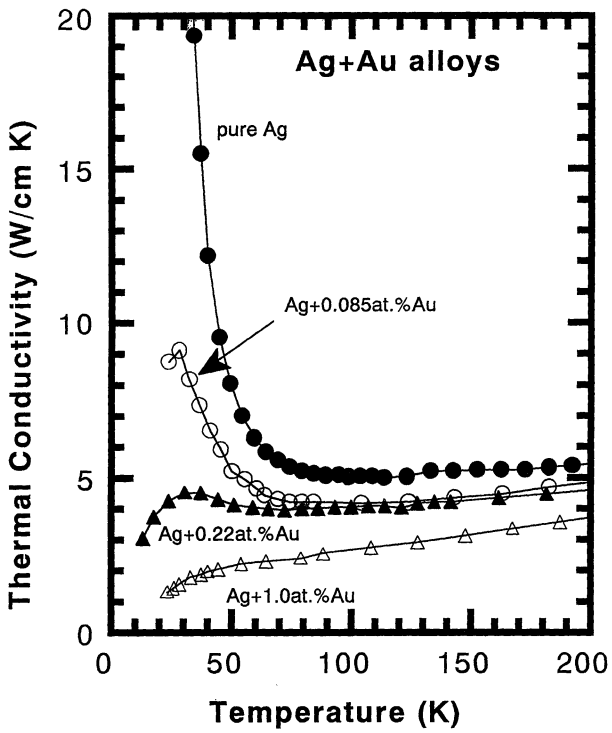


Fig. 2. The temperature dependence of the thermal conductivity of Ag tapes doped by Au at several concentrations.[14]

ly decreases below 20 K. The corresponding increase and decrease of $\kappa(T)$ can also be seen for #10A, but the temperature variation is more moderate with a rather broad maximum near 30 K. This temperature at the observed $\kappa(T)$ maximum ($T_{max}$) is too low for us to assume that the maximum is due to the superconductivity of Bi2212. In oxide superconductors, $T_{max}$ is observed and expected to occur above $T_c/2$. The anomalous behavior of the present specimens should be attributed to Ag doping because the anomaly becomes more remarkable with increasing amount of doped Ag.

Previously, we measured the thermal conductivity of Ag+Au alloy tapes with various concentrations of Au.[14] Figure 2 shows examples of $\kappa(T)$ of several Ag+Au tapes. We notice that, in accord with the general behavior of the thermal conductivity of metals,[15] $\kappa(T)$ of relatively pure Ag+Au alloy tapes shows the maximum at around 20–30 K. Comparing Fig. 1 with Fig. 2, we notice that $\kappa(T)$ of #15A is qualitatively similar to that of Ag+0.085 at.% Au tape and $\kappa(T)$ of #10A to that of Ag+0.22 at.% Au tape. We assume that the enhancement of $\kappa(T)$ of #15A and #10A compared to undoped #00A is entirely due to added Ag and analyze the temperature and Ag content dependence of $\kappa(T)$ of Ag-doped specimens on a simple model.

The present FZ-Bi2212 samples consist of rather large grains (≈mm in the ab-plane), and doped Ag in the shape of particles may locate either at grain boundaries or inside the grains with certain probabilities. Ag particles situated in the boundaries tend to link with each other and may efficiently contribute to the formation of a kind of "linked heat path" of Ag particles. In contrast, the Ag particles inside the grain tend to be isolated from each other. Figure 3(a) shows a model picture of the grains and the boundaries of the Ag-doped specimen in a cubic shape. We approximate the complex heat path in Fig. 3(a) by the simple path configuration shown in Fig. 3(b). In Fig. 3(b), Ag particles which contribute to the "linked heat path" are collected to form Ag pillars of twelve cubic sides, and the Ag particles inside the grain are collected to form a smaller "in-

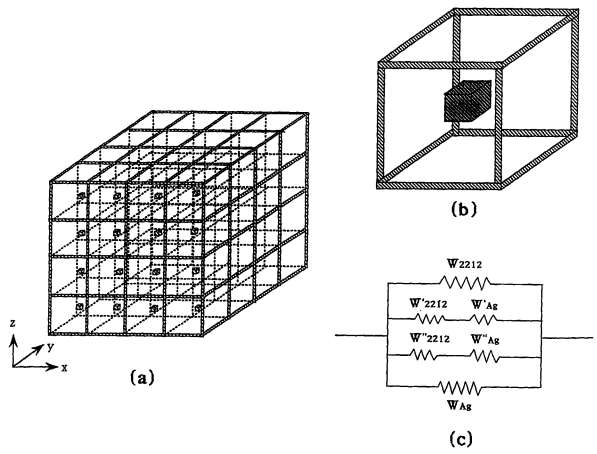


Fig. 3. (a) A schematic picture of the grains and grain boundaries of Ag-doped Bi2212 crystals. Ag particles are located at either "linked heat path" sites in the grain boundaries or isolated sites inside the grains. (b) A simplified model used in the present analysis. Ag particles in the "linked heat path" are collected to form 12 cube side pillars, and Ag particles in the grains to form a smaller inside cube. (c) Equivalent circuit used to calculate the conductivity of the model cube in (b).

side cube''. A generalized heat path circuit corresponding to the configuration in Fig. 3(b) is given by Fig. 3(c). If the Ag volume fractions contributing to the ''linked heat path'' and to the ''inside cube'' are $x$ and $y$, respectively, and the Ag weight fraction in the specimen is $z$ (wt%), then the total thermal resistance W of the heat circuit in Fig. 3(c) is given by

$$W=\frac{1}{\frac{1}{W_{2212}}+\frac{1}{W'_{2212}+W'_{Ag}}+\frac{1}{W''_{2212}+W''_{Ag}}+\frac{1}{W_{Ag}}} \quad (1)$$

where $W_{2212}$ is the thermal resistance of the path through the Bi2212 component, $(W'_{Ag}+W'_{2212})$ is that of the path including the ''inside cube'', $(W''_{Ag}+W''_{2212})$ is that of the path crossing the ''linked heat path'', and $W_{Ag}$ is that of the path along the ''linked heat path''. If one side length of the sample cube is $a$, that of the ''inside cube'' is $b$ and that of the cross section of the ''linked heat path'' is $c$, each thermal resistance component is represented as $W_{2212}=a/[\kappa_{2212}(a-b-2c)(a+b-2c)]$, $W'_{2212}=(a-b)/(\kappa_{2212}b^2)$, $W'_{Ag}=1/(\kappa_{Ag}b)$, $W''_{2212}=1/(4\kappa_{2212}c)$, $W''_{Ag}=1/(2\kappa_{Ag}(a-2c))$ and $W_{Ag}=a/(4\kappa_{Ag}c^2)$. The relations between the values of $a$, $b$, $c$ and $x$, $y$, $z$ are shown in the following:

$$\left(\frac{b}{a}\right)^3\left(\frac{x}{y}\right)=12\left(\frac{c}{a}\right)^2-16\left(\frac{c}{a}\right)^3 \quad (2)$$

$$\left(\frac{b}{a}\right)^3=\frac{1}{\left[\left(\frac{100}{z}-1\right)\frac{\rho_{Ag}}{\rho_{2212}}+1\right]\left(\frac{x}{y}+1\right)}, \quad (3)$$

where $\rho_{Ag}$ and $\rho_{2212}$ indicate the densities of the silver and the Bi2212 mother material, respectively. By using the measured thermal conductivities of #00A as $\kappa_{2212}$ and of Ag+0.085 at.%Au tape as $\kappa_{Ag}$ for #15A and of Ag+0.22 at.%Au tape as $\kappa_{Ag}$ for #10A, $x$ and $y$ values were determined so as to get the best fitting between the experimental and calculated $\kappa(T)$ values. The results of the fitting are shown in Fig. 4(a) for #15A and Fig. 4(b) for #10A, respectively. For #15A the ratio $x/y$ was determined to be 0.75, while $x/y=0.85$ was obtained for #10A. These x/y ratios of nearly 1 suggest that a considerable part of the doped Ag contributes to the ''linked heat path''. If we assume that the ''linked heat path'' mainly occurs along the grain boundaries, doped Ag particles tend to locate very strongly at the boundaries because the effective volume fraction of the boundary in the whole sample should be by far smaller than that of the grain. Furthermore, in actual cases, not all Ag particles in the boundaries contribute to the ''linked heat path''. The present model also counts the isolated Ag particles in the boundary as a part of the ''$y$'' fraction contributing to the inner isolated cube. Thus the $x/y$ ratio should stand for the minimum value of Ag particles in the boundaries. The somewhat larger value of $x/y$ of #10A compared to that of #15A may suggest that at the initial doping of a small amount of Ag, Ag particles even more strongly prefer boundary sites to intragrain sites. It is also worthwhile to note that the threshold value of three-dimensional percolation is 0.16 in terms of the volume fraction of the impurity phase. Even Bi2212+15 wt%Ag (#15A) corresponds to 9% volume fraction of Ag, which is well below the threshold value, and the formation of a linked Ag path

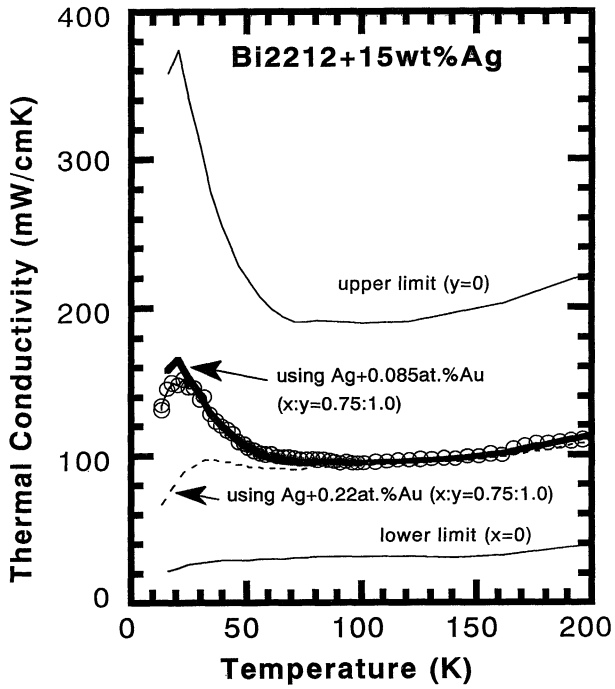


Fig. 4. (a) The best-fitting curve and the upper and lower limits of $\kappa(T)$ for the Bi2212+15 wt%Ag sample calculated by use of the conductivity data of the Ag+0.085 at.%Au tape. The broken line shows the fitting curve obtained by use of the data of the Ag+0.22 at.%Au tape for comparison.

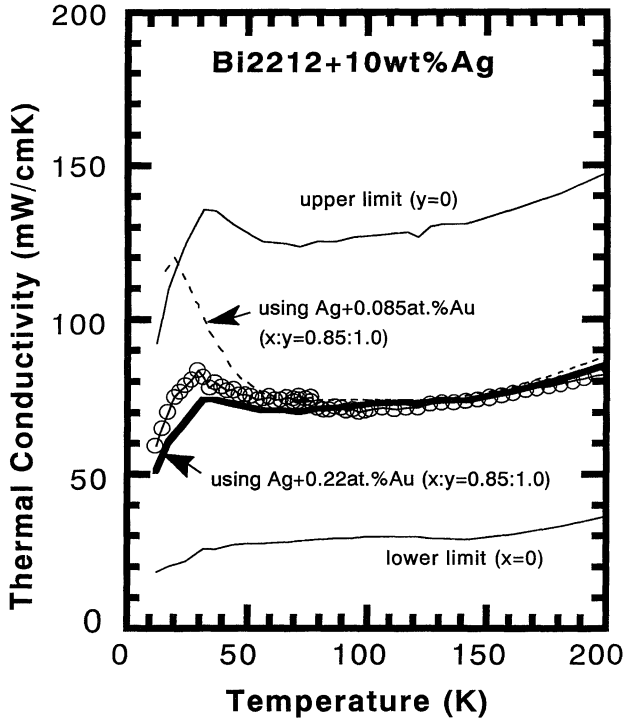


Fig. 5. (b) The best-fitting curve and the upper and lower limits of $\kappa(T)$ for the Bi2212+10 wt%Ag sample calculated by use of the conductivity data of the Ag+0.22 at.%Au tape. The broken line shows the fitting curve obtained by use of the data of the Ag+0.085 at.%Au tape for comparison.

cannot be expected on the basis of the random percolation theory.[16]

In Figs. 4(a) and 4(b), we notice that the use of Ag+0.085 at.%Au tape data for $\kappa(T)$ fitting of #15A leads to a slightly higher maximum than the observed value, while the use of Ag+0.22 at.%Au data for #10A results in a slightly lower maximum. As is well known,[15] and as one can see in Fig. 2, the maximum value of the thermal conductivity of metals strongly depends on the purity and becomes larger with higher purity. As summarized in Table I, the residual resistance ratio ($RRR$) of Ag+0.085 at.%Au is 37 and that of Ag+0.22 at.%Au is 15. If we use the $\kappa(T)$ curve of Ag metal with $RRR \approx 30$ for #15A and the $\kappa(T)$ curve of Ag with $RRR \approx 20$ for #10A, a better fitting is possible for both cases. However, the correction of the $x/y$ ratio caused by this change of $RRR$ value is small and not so meaningful for the present rather rough estimation. This is because the conductivity of Ag at high temperatures ($T \geq 80$ K) is only slightly influenced by the minor change of $RRR$, and the present fitting has been performed in the range $T \geq 80$ K. The present analysis indicates that Ag particles in #15A are purer than those in #10A, which is in agreement with our intuition since the thicker Ag heat path in more heavily Ag-doped #15A may be comparatively immune from impurity contamination in the Bi2212 mother compound.

In Figs. 4(a) and 4(b), the upper limit ($y=0$) and the lower limit ($x=0$) of the $\kappa(T)$ estimation based on the present model are also represented. In this model analysis, we tentatively assumed that the heat path formation is isotropic. In view of the layered crystal structure of the Bi2212 mother compound, this assumption should be examined by measuring the thermal conductivity along the $c$-axis, which we could not accomplish because of the limited sample dimension along the $c$-axis. If we emphasize the two-dimensional structure of the oxide suprconductors, the four Ag pillars in the $c$-direction should be removed from the model cube in Fig. 3(b). This independent layer model gives the ratios $x:y=0.45:1.0$ for #10A and $x:y=0.40:1.0$ for #15A.

## 4. Conclusions

A phenomenological model based on a generalized circuit was proposed to handle the transport phenomena in macroscopically inhomogeneous media and applied to the thermal conductivity analysis of Bi2212+15 wt%Ag and Bi2212+10 wt%Ag crystals. The results are summarized as follows

(1) A simple model which distributes the doped silver in grain boundaries and inside the grain reproduced the observed enhancement and the temperature dependence of $\kappa(T)$.

(2) The ratios of Ag in the boundaries to that inside the grains were determined to be 0.75:1.0 for Bi2212+15 wt%Ag and to be 0.85:1.0 for Bi2212+10 wt%Ag. Doped Ag particles are preferentially located at the boundaries.

(3) The residual resistivity ratio ($RRR$) of Ag particles in Bi2212+15 wt%Ag is about 30 and that in Bi2212+10 wt%Ag is about 20.

## Acknowledgements

The authors wish to thank T. Naito and S. Oikawa of Iwate University for their assistance with the measurements and the calculation of thermal conductivity.

1) N. Imanaka, F. Saito, H. Imai and G. Adachi: Jpn. J. Appl. Phys. **28** (1989) L580.
2) M. K. Malik, V. D. Nair, A. R. Biswasand, R. V. Raghavan, P. Chaddah, P. K. Mishra, G. R. Kumar and B. A. Dasannacharya: Appl. Phys. Lett. **54** (1989) 766.
3) Y. Matsumoto, J. Hombo and Y. Yamaguchi: Appl. Phys. Lett. **56** (1990) 1585.
4) S. X. Dou, K. H. Song, H. K. Liu, C. C. Sorrell, M. H. Apperler and N. Savvides: Appl. Phys. Lett. **56** (1990) 493.
5) Y. H. Kao, Y. D. Yao, L. Y. Jang, F. Xu, A. Krol, L. W. Song, C. J. Sher, A. Darovski, J. C. Phillips, J. J. Simmins and R. L. Snyder: J. Appl. Phys. **67** (1990) 353.
6) M. Matsukawa, F. Tatezaki, K. Noto, H. Fujishiro, M. Ikebe, K. Michishita and Y. Kubo: submitted to Cryogenics.
7) Y. Kubo, K. Michishita, N. Shimizu, Y. Higashida, H. Yokoyama, Y. Hayami, E. Inukai, A. Saji, N. Kuroda and H. Yoshida: Jpn. J. Appl. Phys. **28** (1989) L1936.
8) K. Michishita, N. Shimizu, Y. Sugawara, W. Ito, Y. Sasaki, Y. Kubo, S. Nagaya and T. Inoue: Jpn. J. Appl. Phys. **32** (1993) L572.
9) N. Shimizu, K. Michishita, Y. Hayami, K. Hattori, Y. Kubo, A. Saji and H. Yoshida: Cryo. Eng. **25** (1990) 71 [in Japanese].
10) N. Hobara, M. Matsukawa, N. Matsuura, H. Fujishiro and K. Noto: Cryo. Eng. **28** (1993) 688 [in Japanese].
11) A. Jezowski, J. Mucha, K. Rogachi, R. Horyn, Z. Bukovski and M. Horobiowski: Phys. Lett. **122** (1987) 431.
12) C. Uher and A. B. Kaiser: Phys. Rev. B **36** (1987) 7135.
13) S. D. Peacor, J. L. Cohn and C. Uher: Phys. Rev. B **43** (1991) 8721.
14) H. Fujishiro, M. Ikebe, K. Noto, T. Sasaoka and K. Nomura: Cryogenics **33** (1993) 1086.
15) E. W. Collings: *Applied Superconductivity Metallurgy and Physics of Ti-Alloys* (Plenum, London, 1986) Chap. 6, p. 252.
16) I. Webman, J. Jortner and M. Cohen: Phys. Rev. B **14** (1976) 4737.